Hyperspectral imaging of macroinvertebrates – a pilot study for detecting metal contamination in aquatic ecosystems

Salmelin Johanna*[1], Pölönen Ilkka[2], Puupponen Hannu-Heikki[2], Hämäläinen Heikki[1], Karjalainen Anna K[1], Väisänen Ari[3], Vuori Kari-Matti[4,5]

[1]University of Jyväskylä, Department of Biological and Environmental Science, P.O. Box 35, FI-40014, University of Jyväskylä, Finland
[2]University of Jyväskylä, Department of Mathematical Information Technology, P.O. Box 35, FI-40014, University of Jyväskylä, Finland
[3]University of Jyväskylä Department of Chemistry, P.O. Box 35, FI 40014 University of Jyväskylä, Finland
[4]Finnish Environment Institute Laboratory Centre/Ecotoxicology and Risk Assessment, Survontie 9 A, FI-40500 Jyväskylä, Finland
[5]Lappeenranta University of Technology, South Karelia Institute, PO Box 20, FI-53851 Lappeenranta, Finland

* Corresponding author
johanna.k.salmelin@jyu.fi
johanna.salmelin@gmail.com
ORCID: 0000-0001-8419-6634
tel. +358405642099

Abstract
The applicability of spectral analysis in detection of freshwater metal contamination was assessed by developing and testing a novel hyperspectral imaging (HSI) application for aquatic insect larvae (Trichoptera: Hydropsychidae). Larvae were first exposed to four different cadmium (Cd) concentrations: 0, 1, 10 and 100 μg L^{-1} for 96 h. Individual larvae were then preserved in ethanol, inspected with microscopy for the number of anomalies in larval gills, and imaged by hyperspectral camera operating with wavebands between 500 and 850 nm. Three additional larvae from each exposure were analyzed for tissue Cd concentration. Although the larval tissue Cd concentrations correlated positively with actual water concentrations, the toxicity response of larvae i.e. frequency of gill abnormalities did not differ among the Cd concentrations. In contrast, hyperspectral imaging data indicated some concentration-response relationship of larval spectral properties to the Cd exposure, but it was too weak for reliable automatic distinction between exposed and unexposed larvae. In this pilot study a workflow for data processing for a novel application of hyperspectral imaging was developed. Based on the results of this preliminary study, the workflow in the imaging process will be optimized and its potential for detecting metal contamination of aquatic environments reassessed.

Keywords: Aquatic insect larvae; cadmium toxicity; Fabry-Perot interferometer; hyperspectral imaging; metal pollution

Acknowledgements
This study was funded by the Finnish Funding Agency for Innovation, TEKES (grant number 40255/11). We thank Rauni Kauppinen from the Finnish Environment Institute for technical assistance.

Introduction

Metal pollution threatens aquatic ecosystems worldwide. High metal concentrations are found especially in stream ecosystems contaminated by effluents from active or abandoned mines, industrial waste waters or drainage waters from acid sulfate soils (Ljung et al. 2009; Byrne et al. 2012). Metal exposure impairs physiological function and reproduction of aquatic organisms (Boening 2000; Pane et al. 2003), and causes adverse health effects in humans (Järup and Åkesson 2009).

Direct measurement of chemical concentrations in water is expensive, as due to typically high spatial and temporal variation, extensive sampling would be required to reliably detect also critical peak concentrations. Moreover, and perhaps more importantly, metal concentrations in the water do not directly indicate the concentrations accumulated in organisms or in food webs. Developing and improving biotesting of effluents and their effects could enable efficient detection of and rapid response to possible pollution incidents (Bae and Park 2014).

Hyperspectral imaging (HSI) is spectroscopy coupled with imaging. The basic principle in spectroscopy is that each substance reflects and absorbs different wavelengths of light. Consequently, a given substance often has a unique spectral signature – a fingerprint. In spectral analysis, the goal is to differentiate and recognize substances based on their spectral properties. HSI diverges from conventional reflectance spectroscopy in that it produces an image of pixel spectra. The technique enables revealing changes, which might be unseen for human eye. HSI has many applications e.g. in geology, mineralogy, agriculture and steel industry including automated detection of metal content (Antonucci et al. 2012; Gutierrez et al. 2010; Riaza et al. 2011). In this study, we attempt to apply – to our knowledge for the first time – HSI in detection of metal contamination in animals, more specifically in aquatic insects. This approach could provide a novel method for quantifying heavy metal pollution in natural water bodies through HSI and spectral data processing. If HSI proves to be a suitable method to differentiate between metal contaminated and non-contaminated larvae, it can be used to replace or support direct measurement of metal concentrations in waters affected by mines and mills and in assessment of associated ecological risk.

Benthic macroinvertebrates are an integral constituent of the aquatic ecosystems and essential to the system functioning (Covich et al. 2004). Furthermore, as an important food source for benthivorous fish, benthic macroinvertebrates may transfer contaminants to higher trophic levels. Larvae of caddisfly family Hydropsychidae are abundant and widespread in running waters. Metal exposure of Hydropsychidae larvae can result in morphological damages such as anal papillae and tracheal gill darkening and reduction, the incidence of which can be used for indication of metal contamination (Leslie et al. 1999; Vuori 1994, 1995; Vuori and Kukkonen, 1996).

The main purpose of this study was to evaluate the applicability of HSI in detecting metal contamination of *Hydropsyche pellucidula* (Trichoptera: Hydropsychidae) larvae with cadmium (Cd) as a representative model compound. Cd is one of the priority hazardous substances in the US and EU legislation (CWA 2002; European Union 2013). Cadmium is mainly released locally into the environment from mining activity as a by-product from zinc (Zn), copper (Cu) and lead (Pb) ore mining (European Environment Agency 2011). Other sources of Cd include industry and agriculture. Many metals like iron (Fe), Zn and Cu are essential to biochemical function of animals, but Cd have no known metabolic function and is highly toxic for plants and fish (Gallego et al. 2012; Mebane et al. 2012). The sensitivity of insect larvae to Cd varies across different taxa (Cain et al. 2004; Buchwalter et al. 2008) and family Hydropsychidae is considered quite tolerant (Mebane et al. 2012). Cd is known to accumulate to insect larvae, but the high variability in the bioconcentration factor (BCF) values, and the observed negative correlation between the exposure and the BCF indicate that BCF is not necessarily an optimal measure for Cd bioaccumulation (Poteat et al. 2012). We assume that metal exposure induces morphological changes, including color alteration, in larvae, and that these changes can be quantified by analyzing larval spectral properties, even better than by more subjective, traditional microscopic observation by humans. In addition, spectral analysis operating also in the wavebands of infrared light might reveal changes invisible to human eye.

Specific issues addressed were: 1) can HSI be used to differentiate between Cd contaminated and non-contaminated larvae? and 2) can metal body burden in Hydropsyche larvae be predicted from hyperspectral data? The larvae were also screened microscopically to explore if they showed any visible morphological abnormalities in response to Cd exposure, and to compare these results with HSI data.

Methods and materials

Test organism and exposure set up

Fifth instar larvae of *Hydropsyche pellucidula* (Trichoptera: Hydropsychidae) were collected from unpolluted River Siikakoski, Finland in November 2012. R. Siikakoski is an appropriate reference site with a demonstrated high ecological and good chemical status (Finnish Environment Institutes Water Quality Database Hertta). Median water pH in R. Siikakoski was 7.0 (range 6.6–7.3) and total hardness (Ca + Mg) 0.2 mmol L^{-1} during 2000 – 2013. Cd concentration in the R. Siikakoski measured during 2003 – 2004 ranged between 0.05 and 0.25 µg L^{-1}. Larvae were transported in aerated river water to the laboratory, where the animals were acclimatized slowly to the test temperature (19 ± 1°C) and test water, kept with photoperiod of light:dark 16:8 h, and fed with aquarium fish flake food Tetramin® ad libitum. Only viable animals after 14 d acclimation period were chosen for the exposures. Animals were not fed during the exposure, or one day prior to the experiment to reduce the amount of fecal material and possible metal sorption to it during the experiment.

The test design included one control and three different exposure concentrations each in three replicates. One replicate consisted of 11 larvae in one test container, a 2 L borosilicate glass beaker, and total number of exposed individuals was hence 132. Test concentrations of Cd were 0.0 µg L^{-1} (control), 1.0 µg L^{-1}, 10.0 µg L^{-1} and 100.0 µg L^{-1}. Volume of experimental water was 0.15 L per larvae. Glass beakers and all vessels and pipets were washed with acid (10% HCl), and then rinsed and soaked in MilliQ water before the exposure. During the exposure, glass beakers were continuously aerated to maintain rapid water circulation and oxygen saturation, and were covered with Parafilm® to prevent water evaporation. In each test vial, artificial plastic substrate was provided for larvae for net spinning. Exposure time was 96 h.

Experimental water and chemicals

Artificial freshwater prepared according to the standard ISO 6341 (1996) ($CaCl\cdot 2\,H_2O$, $MgSO_4\cdot 7\,H_2O$, $NaHCO_3$, KCl) with total hardness (Ca + Mg) of 0.5 mmol L^{-1} was used in all the exposures, prepared into a MilliQ-water, and buffered prior to exposures with 0.5 M phosphate buffer ($Na_2HPO_4\cdot H_2O$, $Na_2H_2PO_4\cdot H_2O$) to pH 7 ± 0.1. After buffering, water was aerated overnight and pH adjusted with 1 M HCl, if needed. Stock solutions of 10 000 mg L^{-1}, 1000 mg L^{-1} and 100 mg L^{-1} were prepared into a MilliQ-water from anhydrous cadmium chloride, $CdCl_2$

(Alfa Aesar GmbH & Co.KG), and test concentrations were prepared by dilution of the stock solution to 5000 ml of test water, which was partitioned as 1650 ml into each glass beaker. Based on the results of a preliminary exposure with similar test setup, Cd concentration of experimental water decreases rapidly due to animal uptake. In order to maintain actual Cd concentrations ≥ 90% of the nominal, experimental water was completely changed at 3 h, 9 h, 24 h, 48 h and 72 h of test duration by decanting. Water samples (50 ml) for Cd analysis from each test concentration and control (n = 4) were taken two times right after test solutions had been prepared to see pipetting accuracy in spiking, and just before each water renewal, preserved with supra pur nitric acid (65% HNO_3) and stored in the refrigerator prior to analyses. Water samples before water renewals at 3 h, 9 h and 24 h were taken only from the first replicate from the control and each exposure concentration, but at 48 h and 96 h water samples were taken from all replicates. pH, temperature (°C) and oxygen saturation (%) were measured daily from each replicate.

Measured end points

Larval mortality was checked daily. After the exposure, one larva per replicate (n = 3 per Cd concentration) was rinsed quickly to remove Cd adsorbed on *H. pellucidula* cuticula with pH-buffered artificial freshwater, weighed and freeze-dried for tissue Cd concentration analysis. All other ten larvae were preserved in 70% ethanol (purity 91.2%) for examination of gill damages and for HSI. Gill examination or HSI imaging results were not acquired from larvae which were prepared into Cd tissue analysis. In the present study, we measured larval wet weight, but according to another study conducted in our laboratory, the mean wet weight to dry weight ratio for *H. pellucidula* larvae (n = 74) is 3.61 (± 0.50) (Ruuth 2017), which may be used as an estimate of conversion factor for tissue concentrations. Hydropsychid gill abnormality index (HY-index, HYI) (Vuori and Kukkonen 2002) was calculated as HYI = $\sum NAG / n$, where *NAG* is the number of abnormal gills, and *n* is the number of individuals. HYI values can vary from 0 to 19 as *H. pellucidula* has 9 pairs of abdominal gill tufts with one extra gill on the 2nd abdominal segment. Normal, undamaged gills are whitish and branching as shown in the picture in Online Resources 1 (ESM 1). A gill tuft was considered damaged, if it was totally reduced or darkened with its basal or distal parts, or if the gill tuft had dark spots on > 50% of its branches (Ratia et al. 2012). Hyperspectral images were taken from ethanol-preserved larvae (n = 120) from their dorsal, ventral, left and right sides. Larvae were individually immersed in tap water and placed with insect needles on a Petri dish just before imaging. Petri dishes were placed on a grey background and larvae imaged in a random order. Normality of the HYI distribution was tested using Shapiro-Wilk-test and equality of variances by Levene test. 1-way ANOVA was used to test if the HYI values differed across exposure concentrations. Spearman correlation was used to study larval Cd concentration in relation to actual water Cd concentrations. IBM SPSS Statistics 20 software was used in statistical analyses.

Cd analyses

Weighed and freeze-dried *H. pellucidula* samples were pre-treated for elemental analysis using an ultrasound-assisted digestion method. The samples were digested using 2 mL of aqua regia as a digestion solution. The digestion solution was added, after which sample vessel was closed and placed into a 35 kHz, model Sonorex RK 512 CH ultrasonic water bath supplied by Bandelin. The ultrasound-assisted digestion procedure was carried out in a temperature of about 60 °C. The optimized sonication procedure lasted 15 minutes, divided into five equal steps. The sample vessel was shaken by hand between each step to ensure effective mixing of the sample and the digestion solution. After cooling, the sample solution was transferred into a volumetric flask and diluted to a final volume of 10 ml with water. All the ICP-OES measurements (larval tissue and water samples of 10 and 100 μg L^{-1}) were performed with a Perkin-Elmer (Norwalk, CT, USA) model Optima 8300 inductively coupled plasma optical emission spectrometry. A cyclonic spray chamber and GemCone Low-flow nebulizer were used throughout. The determination of Cd concentrations was performed using parameters of the instrument (nebulizer flow 0.6 L min^{-1}, auxiliary gas flow 0.2 L min^{-1}, plasma gas flow 8 L min^{-1} and plasma power of 1450 W). Two wavelengths with the axial plasma viewing used in the determination were 228.802 nm and 214.440 nm. A Perkin Elmer Model AAnalyst 800 atomic absorption spectrometer with an AS-800 autosampler was used for GFAAS measurements in order to perform accurate analysis of Cd at low level of concentrations (water samples of 0 and 1 μg L^{-1}). All the measurements were based on integrated absorbance and were performed using a Zeeman-effect background correction system. The determination of Cd was performed at 228.8 nm using a Perkin Elmer hollow cathode lamp supplied by Perkin Elmer. Pyrolytic graphite-coated THGA tubes with end caps and an integrated L‘vov-type platform (Perkin Elmer) were used. Argon (AGA, Espoo, Finland) was used as a protective gas throughout. 20 μL of sample solution and 5 μL of matrix modifier solution (a mixture of 0.1% $NH_4H_2PO_4$ + 0.06% $Mg(NO_3)_2$) were injected into the furnace. All the ICP-OES measurements were carried out using a four-point calibration. The determination of Cd was performed by taking the most sensitive emission lines to attain the sensitivity required. The detection limits of the determination of water samples using wavelengths 228.802 nm and 214.440 nm resulted in 0.69 and 0.76 μg L^{-1}, respectively. The detection limit for the *H. pellucidula* tissue samples using same wavelengths resulted in 0.15 and 0.16 mg kg^{-1}. All the GFAAS measurements were done using a six-point calibration. The characteristic masses for each analysis were calculated by the measurement of 2.5 μg L^{-1} of Cd standard solution. The characteristic masses calculated were within 10% of the recommended values. The detection limit of the determination of Cd in water samples by GFAAS resulted in concentration of 0.23 μg L^{-1}. The accuracy of the method was tested by the analysis of SRM1643f (Trace elements in water) and DOLT-4 (Dogfish Liver) certified reference materials. The determination of Cd resulted in recovery rates from 95.6% to 99.5% for both of the CRMs analyzed.

Hyperspectral imaging

The main instrument used was a compact and lightweight hyperspectral imager developed by VTT Technical Research Centre of Finland. Spectral separation in this device is based on the piezo-actuated Fabry-Perot interferometer (FPI). The component is hermetically sealed into a metal can filled with nitrogen. Both the parallelism and the distance between the mirrors of the Fabry-Perot interferometer need to be controlled with great degree of accuracy. This is achieved with three closed loop control systems positioned at the edges of the mirror plates. Each channel has a piezoelectric actuator with associated capacitive measuring element, which is used to determine the mirror separation. Each channel is controlled with nanometer accuracy to obtain the desired parallelism and air gap between the mirrors. Detailed information about camera is given in Table 1.

Table 1 Specifications of VTT's Fabry-Perot hyperspectral imager.

Parameter	
Horizontal and vertical FOV (deg.)	> 36 > 26
Nominal focal length (mm)	9.3 ± 3 (Custom lenses)
Wavelength range (nm)	500–885
Spectral resolution at FWHM (nm)	9–40
Adjustable spectral resolution step	< 1
f-number	< 6.7
Maximum spectral image size (pixels)	2592 × 1944
Spectral image size with default binning (pixels)	320 × 240
Camera dimensions (mm)	62 × 66 × 219
Weight (g)	< 450

In imaging setup HSI was mounted to a stand using a macro objective for sufficient magnification. Illumination was provided from both sides using one 200 W broadband halogen light on each side of the specimen holder. This lighting setup was selected to provide even light distribution over the subject without significant shadows. Imaging system setup is illustrated in Online Resources 2 (ESM 2). Incandescent light sources were utilized to provide a broadband illumination spectrum without significant spikes or other abnormalities. Each larva was prepared and mounted with non-reflective matte black metal pins prior to imaging using the same exposure and integration period settings, with the same sequence of spectral bands for all specimens. In our experiment, we used default spatial pixel binning, which improved noise performance of imaged spectra. Water level in the specimen holder was maintained at a level sufficient to fully immerse each specimen to prevent any reflective border effects from parts of the specimen disturbing the surface of the water. This also ensured similar additional spectral absorption caused by the water covering the specimen. Further standardizing the depth of this immersion is of importance for achieving as comparable imaging conditions as possible. Petri dish where specimens were set was on diffuse grey surface (approx. 30% reflectance). Used wavelengths and full width at half maximum (FWHM) of each band are listed (Table 2).

Table 2 Used wavelengths and full width at half maximum (FWHM) of each band

Wavelenght	496.2	496.4	499.2	503.2	507.2	510.8	514.6	518.9	523.7	528.4
	532.4	533.5	535.9	538.5	539.6	543.2	547.3	552	557.1	561.8
	566.2	571.5	579.1	582.8	586.1	589.8	593.8	597.7	601.9	606.3
	610.9	612.2	618	625.9	634.1	639.8	646	653.6	659.9	660.8
	666.6	666.9	674.5	682.3	688.9	695.3	701.8	709.1	716.4	723
	729.5	735.6	744	750.5	756.7	762.5	769.8	777.7	786.7	793.4
	800.2	806.2	812.3	818.3	824.9	832.7	838.6	846.5	852.5	859.8
FWHM	32.1	30.3	29.3	45.6	30.2	29.2	30.8	25.2	30.7	20.9
	30.9	31.7	31.2	30.3	30.3	31	30.6	30.7	19.4	29.9
	21.9	30.3	21.4	30.7	21	30.7	21.8	29.4	22.8	29
	23.1	29.4	22	31	20.4	31.9	19.8	31.6	19.8	30.3
	20.2	29.6	21.4	28.5	22.2	28.1	22.4	28.6	21.8	29
	23.3	28.7	24.9	28.3	23	28.6	20.2	27.6	19.2	28.4
	19.7	28.5	19.6	19.5	19.8	20.4	11.2	20	12.9	15.3

A hyperspectral image is a stack of grayscale images (Figure 1). Each of these images represents intensities at a given wavelength of light. A given pixel in each image is from the same target location. Thus, if a vector of pixels is taken through this stack, it forms a spectrum from a given point in the imaged object. After all specimens were imaged with the system, all pixels from all spectral cubes were transformed to one large data matrix so that each row corresponded to a certain spectrum from a certain image. From this matrix unique spectral fingerprints were looked for. These fingerprint spectra are called as endmembers. The occurrence of each endmember can then be computed through inversion. Our assumption was that based on the statistical features for each specimen we could create supervised classification for specimen's contamination. In this case specimens would be classified to four groups based on the exposure concentration.

Our data processing pipeline was:

- Data normalization to reflectance. From each image baseline spectrum s_0 was selected manually. Raw imaging data was converted to reflectance $x = s_{i,j} / s_0$ for all pixels in image, where $s_{i,j}$ is spectrum of a single pixel.
- Spectral unmixing to delineate specimen from image. Vertex component analysis (VCA) was used to detect spectrum of specimen from image. With detected spectrums inversion was calculated using filter vector algorithm (FVA) to create a mask for specimen.
- All spectra from specimen were gathered and endmembers were selected from Figure 2 scatter plot. Endmembers are considered as vertices of convex hull of a data set.
- Inversion for selected endmembers was calculated using FVA and abundance maps were formed.
- For abundance images statistical features were calculated. Features were calculated based on the abundance maps and textures of abundance maps using local binary pattern algorithm. Used statistical features were scale and rotation invariant (average, median, mode, variance, standard deviation, entropy, difference entropy, difference variance, difference standard deviation).
- Manifold learning approach was utilized to classify specimens to different groups. For the manifold learning feature space's dimension was reduced using diffusion maps. For specimens in embedded space k-nearest neigbour (KNN) based classification was used. For cross-validation leave-one-out method was used with KNN.

We will here explain in details how to find the unique spectral fingerprints from the data matrix. We utilized a spectral unmixing method. An assumption behind spectral unmixing is that the spectrum arriving at a given pixel is a mixture of reflections that have been given off from different materials present in the scene being imaged. To effectively separate these materials, a model is required to describe this process, making it possible to devise a reverse operation. One common assumption is a so- called linear mixing model, which assumes the detected spectrum for each pixel to consist of a linear combination of substance- originated constituent spectra, termed as endmembers.

As given in (Keshava 2003), linear mixing model (LMM) for single spectrum can be described as

$$\boldsymbol{x}[\lambda] = \sum_{i=1}^{M} \boldsymbol{a}_i \boldsymbol{s}_i[\lambda] + \boldsymbol{w}[\lambda],$$

where $\boldsymbol{x}$ is the detected spectrum as a function of wavebands λ, $\boldsymbol{a}_i$ is an abundance coefficient for endmember $\boldsymbol{s}$, M is the number of endmembers and $\boldsymbol{w}$ is the noise term. Expanding LMM to all observed pixel spectra, we shall have a matrix form of $X = AS + W$, where $X = [\boldsymbol{x}_1, \boldsymbol{x}_2 \cdots, \boldsymbol{x}_N]^T$ is $N \times d$ matrix, $A = [\boldsymbol{a}_1, \boldsymbol{a}_2, \cdots \boldsymbol{a}_M]$ is $N \times M$ matrix, $S = [\boldsymbol{s}_1, \boldsymbol{s}_2 \cdots \boldsymbol{s}_M]^T$is $M \times d$ matrix and W is $N \times d$ noise matrix.

Goals of unmixing processes are to estimate these constituent spectra, and their relative abundance for each pixel. Given these abundance coefficients, new images displaying the relative occurrence of a given endmember within the scene can be drawn, usually termed as abundance maps.

Unmixing can be done manually projecting data to a lower dimensional space. We used principal component analysis to project specimens spectra to a lower dimensional space, where endmembers were selected. One unsupervised method used to unmix the spectral data is Vertex Component Analysis, as outlined in Nascimento and Bioucas Dias (2005). This method assumes presence of pure pixels S in the input data X, and proceeds by performing iterative orthogonal projections of the data onto subspace spanned by the previously determined endmembers. The extremity of this projection is taken as being the new endmember signature. This process repeats until M endmembers have been extracted.

As such, the assumption of pure pixels existing is a strong one, and not necessarily true in all types of data. For purpose of discovering material differences present within the scene imaged in contrast to finding endmember spectra directly usable for substance identification, the behavior of selecting the most purest pixel spectra as the endmember signatures is often sufficient.

To obtain abundance maps, given spectral datacubes and endmember spectra, two different methods were examined. The first one was a traditional non-negative least squares inversion, which proved to provide good abundance maps, but also is computationally expensive. The other method utilized was the Filter Vector Algorithm (Bowles et al. 1995) (FVA), which in turn provided reduced computational cost.

The FVA forms a set of filter vectors F, which are used to estimate abundance coefficients. Estimation is performed in the following way $A = FX$, where $F = [RS]^{-1}R$ and $R = S^T - (I/N\,S)^T$. Here I is $N \times N$ unit matrix.

Proposed workflow offers us features, which can be utilized in separation of different spectra. In the case of *H. pellucidula* this gave us an opportunity to utilize numerical features based on specimen’s reflectance spectrum.

After unmixing and inversion we calculated scale and rotation invariant statistical features for each specimen. These features were listed earlier. With this feature space we got 54 different features for each specimen, which also means 54 dimensional space. Because of large dimensionality diffusion maps (Coifman and Lafon 2006) were used to reduce it. Diffusion maps is a non-linear dimensionality reduction algorithm, which detects underlying manifolds from the data.

Now each specimen $i = 1,2,\ldots,120$ has a feature vector $x_i^f \in \mathbb{R}^{54}$ and all these feature vectors form a feature matrix $X^f = \left[x_1^f, x_2^f, \cdots, x_{120}^f\right]^T$. Diffusion matrix W is formed using Gaussian heat kernel

$$k_{i,j} = exp^{\frac{\left|x_i^f - x_i^f\right|}{\epsilon}}$$

in every element of the $W_{i,j\in[1,2,\ldots,120]}$. By normalizing $W$with symmetric matrix $D_{i,i} = \sum_{j=1}^{120} W_{i,j}$ we will get Markovian transition matrix $P = D^{-1}W$. After this the conjugate matrix $\hat{P} = D^{1/2}PD^{-1/2}$ is calculated to determine the eigenvalues of P. Now, $\hat{P} = D^{-1/2}WD^{-1/2}$, which is also known as normalized graph Laplacian and it maintains eigenvalues. Singular value decomposition is used to find the singular values φ_i and singular vectors ψ_i. Now, $\Phi_i = \varphi_i\psi_i$ are the coordinates of the embedded data.

After dimensional reduction step, we can use classification algorithm to classify specimens to four different exposure groups. We apply simple three nearest neighbor classification to this using the embedded data Φ and more precisely 2nd, 3rd and 4th eigenvectors and -values. To test accuracy of classification cross-validation scheme is built with a leave-one-out method. In this method, one data point is removed and the rest are used for training the classifier. Now this removed data point is classified with a trained classifier. This procedure is repeated for all the data points.

Results and discussion

Water chemistry remained stable throughout the exposure. Average pH (± SD) was 7.14 (0.03), temperature 18.8 °C (0.3) and oxygen saturation 100.0% (0.6). The actual Cd concentrations in experimental water were slightly over the nominal throughout the exposure at the concentrations of 10.0 and 100.0 µg L^{-1}. At the lowest Cd concentration (1.0 µg L^{-1}) actual Cd concentration was only 48–80% of the nominal concentration despite frequent water renewals.
Larval tissue Cd concentration (µg g^{-1} ww) varied somewhat within treatments (Figure 5), but showed a significant positive correlation with actual water concentrations (µg L^{-1}) ($r_s = 0.75$, $p = 0.005$).
There was no larval mortality in any of the exposure concentrations. HYI showing the average number of damaged gills per larvae in the exposed population was low and varied from 1.47 (± 0.42) in the control to 1.63 (± 0.25) in the exposure concentration of 10.0 µg L^{-1} with no significant differences among exposure populations ($F = 0.077$, df = 3, $p = 0.971$) (Figure 3).
HSI data analysis indicated that larvae exposed to high Cd concentrations might have different spectral properties than control larvae. First of all, different parts of the specimen based on spectral unmixing were able to separate. In Figure 4 is one specimen presented as RGB image (A) and abundances of the found endmembers (B, C, D). It seems that B represents dark parts of the thorax and abdomen. C and D present endmembers for the segments, where tissue is soft and does not include pigment.

Table 3 Average water (µg L^{-1}) and larval tissue (µg g^{-1} ww) Cd concentrations (± SD) during the exposure. Experimental water was completely changed five times (at 3, 9, 24, 48 and 72 h), and exposure duration was 96 h

Time	Nominal water Cd µg L^{-1}	Actual water Cd after spiking µg L^{-1}	Actual water Cd before water renewal µg L^{-1}	Larval tissue Cd µg g^{-1} ww	Larval ww mg
3 h	0.0	> 0.22	> 0.22		
9 h	0.0	> 0.22	> 0.22		
24 h	0.0		> 0.22		
48 h	0.0		> 0.22		
72 h	0.0		> 0.22		
96 h	0.0		> 0.22	0.62 (0.41)	53.3 (4.32)
3 h	1.0	1.88	0.80		
9 h	1.0	1.26	0.85		
24 h	1.0		0.75		
48 h	1.0		0.62		
72 h	1.0		0.48 (0.11)		
96 h	1.0		0.54 (0.05)	3.98 (1.96)	50.27 (8.09)
3 h	10.0	12.00	10.83		
9 h	10.0	12.20	10.98		
24 h	10.0		9.90		
48 h	10.0		10.00		
72 h	10.0		10.35 (0.34)		
96 h	10.0		10.74 (0.13)	12.76 (6.43)	49.17 (1.83)
3 h	100.0	119.70	117.10		
9 h	100.0	123.60	116.90		
24 h	100.0		117.80		
48 h	100.0		121.90		
72 h	100.0		121.10 (2.08)		
96 h	100.0		122.90 (0.54)	8.92 (3.23)	60.17 (7.27)

Classifier gave 32% accuracy, which is better than guessing (25%). The most promising individual set of features, more specifically the inverse of the variance of pixel intensities in a specimen, correlated with the Cd exposure ($r_s = 0.29$) (Figure 5). These data were captured from the dorsal side of the insect. This result can be interpreted as abundance image’s pixel intensities having less difference between each other when Cd exposure concentration is higher. The result indicates that soft parts of the larvae are darker in higher exposure concentrations (Figure 5).

H. pellucidula larvae accumulated waterborne Cd into their tissues in this study. Accumulated Cd concentration reflected the actual water Cd concentrations, but was on average highest at the second highest exposure concentration, 10 μg L^{-1}. There is evidence of active internal Cd concentration regulation and some physiological control seem to exist for protecting insects from excess uptake (Buchwalter et al. 2008; Poteat et al. 2012). Larval body burden represents the bioavailable fraction of metals, not the entire metal exposure in the water, and therefore reflects the potential harmful ecotoxicological effects of metals on biota. In the present study, larval body burden was high compared to Cd tissue concentrations in field-collected larvae of the same family (e.g., Cain et al. 2000; Awrahman et al. 2016; Prommi and Payakka 2018).

All exposure concentrations 1–100 μg L^{-1} used in this study were acutely in a sublethal range for *H. pellucidula* as there was no mortality during this 96 h test. In streams receiving mine drainage, Cd concentration may vary 0.3–2.0 μg L^{-1} (Ramani et al. 2014), but rivers receiving waters from historical deep metal mines can contain < 10–2600 μg L^{-1} Cd (Byrne et al. 2012). In Finnish mine-impacted streams and lakes, Cd concentration has exceeded on a spill occasion the maximum environmental quality standard, MAC-EQS, over tenfold (European Union 2013; Kauppi et al. 2013). Water hardness generally protects against Cd toxicity since calcium (Ca) ions can compete with Cd for binding sites on cell membrane thus preventing Cd uptake (Penttinen et al. 1998). In this study, a soft water characteristic of Finnish water bodies and natural habitats of *Hydropsyche* larvae was used. According to Mebane et al. (2012), larval Arctopsychidae (closely related to Hydropsychidae) were very tolerant for Cd with 96-h EC50 > 458 μg Cd L^{-1} when stream water was used as an experimental water with estimated dissolved organic carbon being 0.6 mg L^{-1} and field measured pH 6.8–7.5. There are differences in Cd sensitivity between insect families reflecting their phylogeny (Buchwalter et al. 2008). *Hydropsyche* spp. are considered metal tolerant with more efficient detoxification processes and accumulated Cd whole-body concentrations in metal polluted sites lower than e.g., in mayfly larvae (Cain et al. 2004). *H. californica* has shown very high Cd elimination rate compared to other aquatic invertebrate taxa (Buchwalter et al. 2008). Also animal size affects metal tolerance. Larger individuals may be more tolerant with decreased surface area:mass ratio compared to smaller individuals with higher ion uptake rates (Poteat and Buchwalter 2014) which makes earlier instar larvae more susceptible to metals. Metal exposure through dietary sources is found to be potentially more toxic than uptake of dissolved metal from water (Xie and Buchwalter 2011).

No differences were observed in the number of gill damages in *Hydrospyche* larvae among the three different Cd concentrations and the control. Overall, the incidence of gill abnormalities was low compared to much higher incidence of gill damage (average HYI 5–15) found by Vuori and Kukkonen (2002) when exposing *H. siltalai* larvae to very high Cd concentrations (160 and 10 000 μg L^{-1}). Although the visual inspection for gill damages did not reveal any relation to Cd concentrations, HSI succeeded to detect a weak correlation between water Cd concentrations and spectral features, showing a relationship between darkening of larval soft tissues and Cd exposure concentration. These features could not be correlated to larval Cd tissue concentration directly since the larvae that were imaged were not suitable anymore for tissue Cd analysis due to ethanol preservation. This correlation and maybe those for some other features might have become stronger if some apparent sources of error could be avoided. Spectral features of the larvae might have been measured better if the larvae were not immersed in water. In the current imaging system, this was required to avoid larvae from drying out under illumination. Because there was a range of larval sizes present, there was additional variance in the level of water surface. Water absorption can be an additional source of error, and would thus be advantageous to eliminate. As the larvae are not flat, the thickness of water layer on them varies among different parts of the larva, and potentially, to some extent among specimens. However, for the wavelengths used in imaging, the absorption by water is limited and has relative small effect on the imaged spectra. Thus, this was handled as a noise factor of linear mixing model, and was thereby controlled for in the data processing. The manual preparation with needles also gives rise to a further uncertainty, as each larva is positioned and stretched out in a slightly different manner, which also affects what areas are imaged and to what extent.

Physiological explanation for the soft tissue darkening in the higher Cd concentrations indicated by HSI is unclear. Vuori (1994) and Vuori and Kukkonen (2002) observed heavy visual darkening of hydropsychid soft tissues at high Cd exposure levels. This phenomenon was associated with heavy darkening and reduction of tracheal gills of the larvae. HSI is known to detect color changes in organisms before the changes are visible to human eye (Little and Summy 2012). By the same token, HSI indication of soft tissue darkening of hydropsychids in the present study may be an early-warning signal of color change related to metabolic disturbances. Cd is observed to alter normal cell ultrastructure in insects, which is linked to protein-based defense system activation (Braeckman et al. 1999a, b). Another explanation may be related to adsorption of Cd on body surfaces. Significant proportion of metals can be adsorbed on the body surfaces of aquatic insects, mainly as oxide coating on the cuticle surfaces (Dittman and Buchwalter 2010) or direct binding to chitin (Hare 1992). The main component of abdominal cuticle of insects is chitin. Number of studies has shown rapid biosorption of Cd to chitin (Gonzalez-Davila et al. 1990; Zhou et al. 2004). The high affinity of chitin to Cd and other metals is related to its structure comparable to the polysaccharide cellulose assembled into crystalline nanofibrils (Vincent 2002). Short-term preservation of larvae in 70% ethanol has probably no significant impact on Cd concentrations. Concentrations of closely related zinc in invertebrates have also been shown to be unaffected by ethanol preservation (Braun et al. 2009).

In this pilot study the feasibility of a novel technique, HSI, was tested to detect metal contamination of aquatic insects, and a workflow for processing hyperspectral data for this kind of an application was developed. The actual imaging process needs further development, especially concerning stabilization of specimens for spectral imaging in a standardized manner without damaging them. Moreover, it is important to improve the study protocol so that individual level information of both tissue Cd accumulation, gill damages, and specific spectral features are acquired. The results show quite large variation in Cd accumulation, and in the spectral features of larvae, so in the future studies it is essential to get both of these parameters from each individual. Reliable estimates of Cd body burden also may require larger sample sizes than used in this study, where only three larvae per treatment were analyzed. Although a relation between metal exposure concentration and a spectral feature was discovered in the data, it proved to be too weak for performing automatic distinction between the exposed and unexposed specimens. Thus the current data set as such is insufficient for directly estimating Cd water or tissue concentrations. Prediction could be potentially performed by similar machine learning methodologies as here was done directly against the observed data. The absolute values of features for each exposure concentration occupy much the same numerical range (Figure 5), making any potential prediction results considerably more uncertain. Still, we consider these preliminary results encouraging enough to study further if HSI has a potential for detection of metal contamination in aquatic insects. To further develop and test HSI to this end, focus in the future studies should focus on set-ups that will enable a standardized manner of larvae preparation for spectral imaging, and will yield accurate dose-response data.

Conflict of Interest: The authors declare that they have no conflict of interest.

References

Antonucci, F., Menesatti, P., Holden, N.M., Canali, E., Giorgi, S., Maienza, A., & Stazi, S.R. (2012). Hyperspectral visible and near-infrared determination of copper concentration in agricultural polluted soils. *Commun Soil Sci Plan*, 43, 1401–141. https://doi.org/10.1080/00103624.2012.670348

Awrahman, Z.A., Rainbow, P.S., Smith, B.D., Khan, F.R., & Fialkowski, W. (2016) Caddisflies *Hydropsyche* spp. as biomonitors of trace metal bioavailability thresholds causing disturbance in freshwater stream benthic communities. *Environ Pollut*, 216, 793–805. http://dx.doi.org/10.1016/j.envpol.2016.06.049

Bae, M.J., & Park, Y.S. (2014). Biological early warning system based on the responses of aquatic organisms to disturbances: A review. *Sci Total Environ*, 466–467, 635–649. https://doi.org/10.1016/j.scitotenv.2013.07.075

Boening, D.W. (2000). Ecological effects, transport, and fate of mercury: a general review. *Chemosphere*, 40, 1335–1351. https://doi.org/10.1016/S0045-6535(99)00283-0

Bowles, J.H., Palmadesso, P.J., Antoniades, J.A., Baumback, M.M., & Rickard, L.J. (1995). Use of filter vectors in hyperspectral data analysis. In: Proc SPIE 2553, 148–157.

Braeckman, B., Brys, K., Rzeznik, U., & Raes, H. (1999a). Cadmium pathology in an insect cell line: ultrastructural and biochemical effects. *Tissue and Cell*, 31, 45–53. https://doi.org/10.1054/tice.1998.0019

Braeckman, B., Smagghe, G., Brutsaert, N., Cornelis, R., & Raes, H. (1999b). Cadmium uptake and defense mechanism in insect cells. *Environ Res*, 80, 231–243. https://doi.org/10.1006/enrs.1998.3897

Braun, M., Simon, E., Fabian, I., & Tothmeresz, B. (2009). The effects of ethylene glycol and ethanol on the body mass and elemental composition of insects collected with pitfall traps. *Chemosphere*, 77, 1447–1452. https://doi.org/10.1016/j.chemosphere.2009.08.051

Buchwalter, D.B., Cain, D.J., Martin, C.A., Xie, L., Luoma, S.N., & Garland, T. (2008). Aquatic insect ecophysiological traits reveal phylogenetically based differences in dissolved cadmium susceptibility. *Proceedings of the National Academy of Sciences*, 105, 8321–8326. https://doi.org/10.1073/pnas.0801686105

Byrne, P., Wood, P.J., & Reid, I. (2012). The impairment of river systems by metal mine contamination: A review including remediation options. *Crit Rev Env Sci Tec*, 42, 2017–2077. https://doi.org/10.1080/10643389.2011.574103

Cain, D.J., Carter, J.L., Fend, S.V., Luoma, S.N., Alpers, C.N., & Taylor, H.E. (2000). Metal exposure in a benthic macroinvertebrate, *Hydropsyche californica*, related to mine drainage in the Sacramento River. *Can J Fish Aquat Sci*, 57, 380–390. https://doi.org/10.1139/f99-260

Cain, D., Luoma, S., & Wallace, W. (2004). Linking metal bioaccumulation of aquatic insects to their distribution patterns in a mining impacted river. *Environ Toxicol Chem*, 23, 1463–1473. https://doi.org/10.1897/03-291

Coifman, R.R., & Lafon, S. (2006). Diffusion maps. *Applied and Computational Harmonic Analysis*, 21, 5–30. https://doi.org/10.1016/j.acha.2006.04.006

Covich, A.P., Austen, M.C., Brlocher, F., Chauvet, E., Cardinale, B.J., Biles, C.L., Inchausti, P., Dangles, O., Solan, M., Gessner, M.O., Statzner, B., & Moss, B. (2004). The role of biodiversity in the functioning of freshwater and marine benthic ecosystems. *BioScience*, 54, 767–775. https://doi.org/10.1641/0006-3568(2004)054[0767:TROBIT]2.0.CO;2

CWA. (2002). Federal water pollution control act (as amended through p.l. 107-303 Nov 27 2002)

Dittman, E.K., & Buchwalter, D.B. (2010). Manganese bioconcentration in aquatic insects: Mn oxide coatings, molting loss and Mn(II) thiol scavenging. *Environ Sci Technol*, 44, 918–9188. https://pubs.acs.org/doi/abs/10.1021/es1022043

European Environment Agency. (2011). Hazardous substances in Europe’s fresh and marine waters. An overview. EEA technical report.

European Union. (2013). Directive 2013/39/EU of the European Parliament and of the Council amending Directives 2000/60/EC and 2008/105/EC as regards priority substances in the field of water policy.

Gallego, S.M., Pena, L.B., Barcia, R.A., Azpilicueta, C.E., Iannone, M.F., Rosales, E.P., Zawoznik, M.S., Groppa, M.D., & Benavides, M.P. (2012). Unravelling cadmium toxicity and tolerance in plants: Insight into regulatory mechanisms. *Environ Exp Bot*, 83, 33–46. https://doi.org/10.1016/j.envexpbot.2012.04.006

Gonzalez-Davila, M., Santana-Casiano, J.M., & Millero, F.J. (1990). The adsorption of Cd(II) and Pb(II) to chitin in seawater. *J Colloid Interface Sci*, 137, 102–110. https://doi.org/10.1016/0021-9797(90)90046-Q

Gutierrez, J., Picon, S., Rodriguez, A., & Girbau, I. (2010). The application of hyperspectral image processing to the steel foundry process. In proceeding of: International Surface Inspection Summit, Wuhan, China 01/2010.

ISO 6341. (1996). Water quality - Determination of the inhibition of the mobility of Daphnia magna Straus (Cladocera, Crustacea) - Acute toxicity test.

Hare, L. (1992). Aquatic insects and trace metals: bioavailability, bioaccumulation and toxicity. *Crit Rev Toxicol*, 22, 327–369. https://doi.org/10.3109/10408449209146312

Järup, L., & Åkesson, A. (2009). Current status of cadmium as an environmental health problem. *Toxicol Appl Pharmacol*, 238, 201–208. https://doi.org/10.1016/j.taap.2009.04.020

Kauppi, S., Mannio, J., Hellsten, S., Nystèn, T., Jouttijärvi, T., Huttunen, M., Ekholm, P., Tuominen, S., Porvari, P., Karjalainen, A., Sara-Aho, T., Saukkoriipi, J., & Maunula, M. (2013). Assessment of the potential impacts on water environment caused by the gypsum pond leakage at the Talvivaara mine (In Finnish). Suomen Ympäristökeskuksen raportteja 11, 1–90.

Keshava, N. (2003). A survey of spectral unmixing algorithms. *Lincoln Laboratory Journal*, 14, 55–78.

Leslie, H.A., Pavluk, T.I., bij de Vaate, A., & Kraak, M.H.S. (1999.) Triad assessment of the impact of chromium contamination on benthic macroinvertebrates in the Chusovaya River (Urals, Russia). *Arch Environ Contam Toxicol*, 37, 182–189. https://doi.org/10.1007/s002449900504

Ljung, K., Maley, F., Cook, A., & Weinstein, P. (2009). Acid sulfate soils and human health - A millennium ecosystem assessment. *Environ Int*, 35, 1234–1242. https://doi.org/10.1016/j.envint.2009.07.002

Little, C.R., & Summy, K.R. (2012). Accurate Spectral Measurements and Color Infrared Imagery of Excised Leaves Exhibiting Gaussian Curvature from Healthy and Stressed Plants. In: Dimitrios Ventzas (Ed.), *Advanced Image Acquisition, Processing Techniques and Applications I* (pp 123–142). InTech, Rijeka.

Mebane, C.A., Dillon, F.S., & Hennessy, D.P. (2012). Acute toxicity of cadmium, lead, zinc, and their mixtures to stream-resident fish and invertebrates. *Environ Toxicol Chem*, 31, 1334–1348. https://doi.org/10.1002/etc.1820

Nascimento, J., & Dias, J. (2005). Vertex component analysis: a fast algorithm to unmix hyperspectral data. *Geoscience and Remote Sensing*, IEEE Transactions on 43, 898–910. 10.1109/TGRS.2005.844293

Pane, E.F., Smith, C., McGeer, J.C., & Wood, C.M. (2003). Mechanisms of acute and chronic waterborne nickel toxicity in the freshwater cladoceran, *Daphnia magna*. *Env Sci Tech*, 37, 4382–4389. https://pubs.acs.org/doi/abs/10.1021/es034317l

Penttinen, S., Kostamo, A., & Kukkonen, J.V.K. (1998). Combined effects of dissolved organic material and water hardness on toxicity of cadmium to *Daphnia magna*. *Environ Toxicol Chem*, 17, 2498–2503. https://doi.org/10.1002/etc.5620171217

Poteat, M.D., & Buchwalter, D.B. (2014). Calcium uptake in aquatic insects: influences of phylogeny and metals (Cd and Zn). *J Exp Biol*, 217, 1180–1186. doi: 10.1242/jeb.097261

Poteat, M.D., Daz-Jaramillo, M., & Buchwalter, D.B. (2012). Divalent metal (Ca, Cd, Mn, Zn) uptake and interactions in the aquatic insect *Hydropsyche sparna*. *J Exp Biol*, 215, 1575–1583. doi: 10.1242/jeb.063412

Prommi, P.O., & Payakka, A. (2018). Monitoring Cadmium Concentrations in Sediments and Aquatic Insects (Hydropsychidae: Trichoptera) in a Stream near a Zinc Mining Area. *Pol J Environ Stud* 27, 2237–2243. DOI: 10.15244/pjoes/78627

Ramani, S., Dragun, Z., Kapetanovi, D., Kostov, V., Jordanova, M., Erk, M., & Hajrulai-Musliu, Z. (2014). Surface water characterization of three rivers in the lead/zinc mining region of northeastern Macedonia. *Arch Environ Contam Toxicol*, 66, 514–528. https://doi.org/10.1007/s00244-014-0012-z

Ratia, H., Vuori, K.M., & Oikari, A. (2012). Caddis larvae (Trichoptera, Hydropsychidae) indicate delaying recovery of a watercourse polluted by pulp and paper industry. *Ecol Indic*, 15, 217–226. https://doi.org/10.1016/j.ecolind.2011.09.015

Riaza, A., Buzzi, J., Garca-Melendez, E., Carre, V., & Müller, A. (2011). Monitoring the extent of contamination from acid mine drainage in the Iberian pyrite belt (SW Spain) using hyperspectral imagery. *Remote Sens*, 3, 2166–2186. doi:10.3390/rs3102166

Ruuth H. 2017. Detecting cadmium exposure from *Hydropsyche pellucidula* (Trichoptera: Hydropsychidae) larvae using hyperspectral imaging and incidence of gill anomalies. Master of Science Thesis, University of Jyväskylä. Department of Biological and Environmental Science, Aquatic Sciences, 32 pp. (in Finnish). Available at: https://jyx.jyu.fi/handle/123456789/55750

Vincent, J.F.V. (2002). Arthropod cuticle: a natural composite shell system. *Composites Part A: Applied Science and Manufacturing*, 33, 1311–1315. https://doi.org/10.1016/S1359-835X(02)00167-7

Vuori, K.M. (1994). Rapid behavioural and morphological responses of hydropsychid larvae (Trichoptera, Hydropsychidae) to sublethal cadmium exposure. *Environ Poll*, 84, 291–299. https://doi.org/10.1016/0269-7491(94)90141-4

Vuori, K.M. (1995). Species-and population-specific responses of translocated hydropsychid larvae (Trichoptera, Hydropsychidae) to runoff from acid sulphate soils in the River Kyrönjoki, western Finland. *Freshwat Biol*, 33(2), 305–318. https://doi.org/10.1111/j.1365-2427.1995.tb01169.x

Vuori, K.M., & Kukkonen, J.V.K. (1996). Metal concentrations in *Hydropsyche pellucidula* larvae (Trichoptera, Hydropsychidae) in relation to the anal papillae abnormalities and age of exocuticle. *Wat Res*, 30(10), 2265–2272. https://doi.org/10.1016/0043-1354(96)00109-1

Vuori, K.M., & Kukkonen, J.V.K. (2002). Hydropsychid (Trichoptera, Hydropsychidae) gill abnormalities as morphological biomarkers of stream pollution. *Freshwat Biol*, 47, 1297–1306. https://doi.org/10.1046/j.1365-2427.2002.00868.x

Xie, L., & Buchwalter, D.B. (2011). Cadmium exposure route affects antioxidant responses in the mayfly *Centroptilum triangulifer*. *Aquat Toxicol*, 105, 199–205. https://doi.org/10.1016/j.aquatox.2011.06.009

Zhou, D., Zhang, L., Zhou, J., Guo, S. (2004). Cellulose/chitin beads for adsorption of heavy metals in aqueous solution. *Wat Res*, 38, 2643–2650. https://doi.org/10.1016/j.watres.2004.03.026

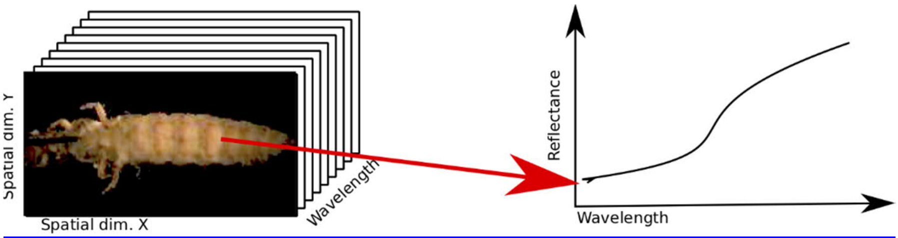

Fig. 1 Illustration of a hyperspectral datacube. Each spatial pixel forms a spectrum through the cube

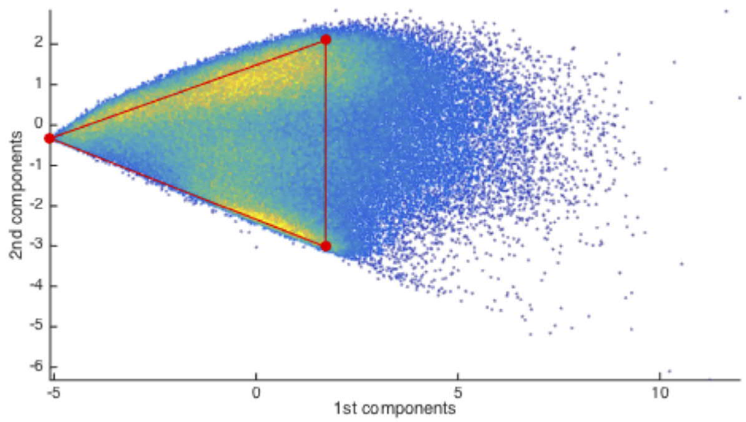

Fig. 2 Illustrative density scatter plot of all the specimen spectra projected to the lower dimensional space with principal component analysis. Projection of the data set is almost convex. Color in scatter plot indicates spatial density of projection. In more yellow (lighter) area there are more scatter points than in blue (darker) area. Majority of the data is between marked three red dots. These dots can be seen as endmembers for the data and data points inside this convex hull can be presented as linear combination of these endmembers. Data points outside of hull consist more noise

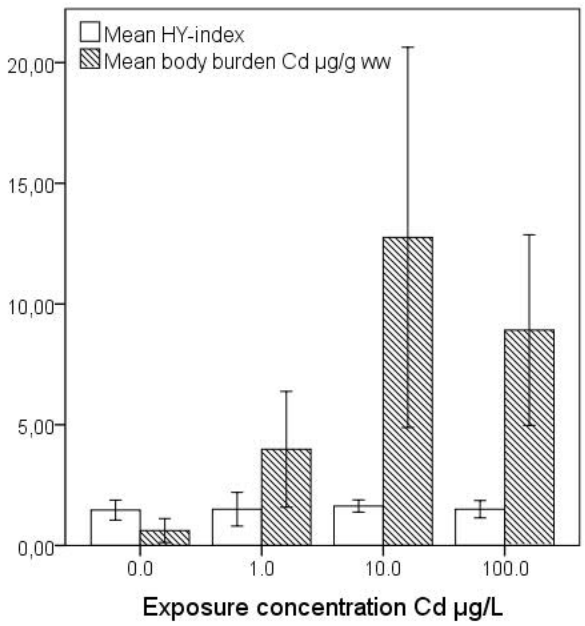

Fig. 3 Mean HY-index (± SD) (n = 30) describing the average number of damaged gill tufts of *H. pellucidula* in the exposed population, and mean larval body burden Cd µg g^{-1} ww (± SD) (n = 3) in Cd-exposure concentrations of 0.0 µg L^{-1} (control), 1.0 µg L^{-1}, 10.0 µg L^{-1}, and 100.0 µg L^{-1}

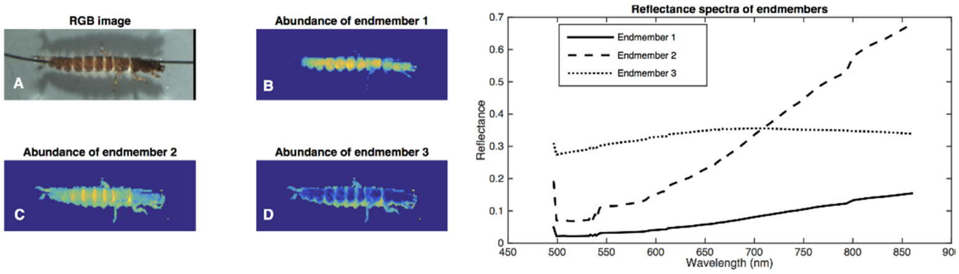

Fig. 4 Separated parts of the specimen based on spectral unmixing. Here is one *H. pellucidula* larvae presented as RGB image (A) and abundances of the found endmembers (B, C, D). Extracted endmembers on the right

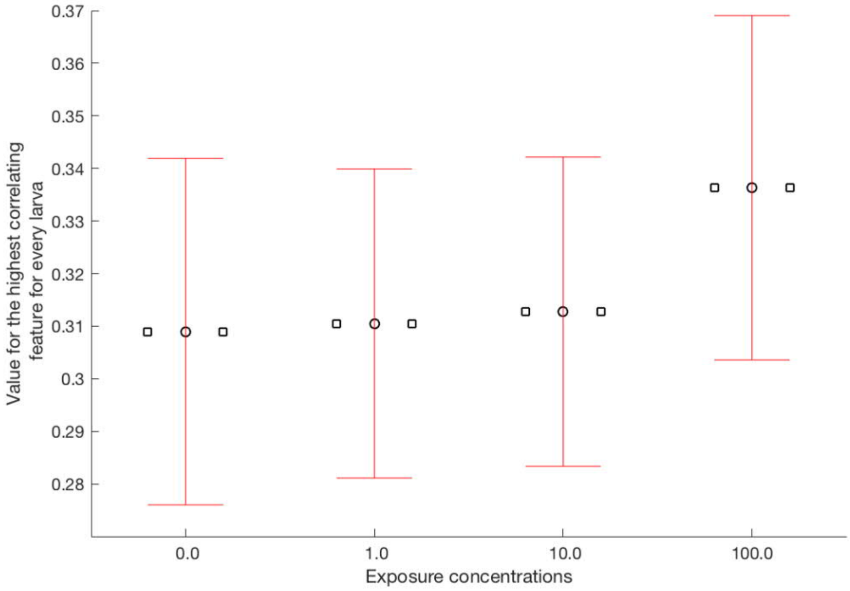

Fig. 5 Values for the highest correlating spectral feature (mean ± SD) for every larva in Cd concentrations of 0 (control), 1, 10, and 100 μg L^{-1}